19th Brazilian Congress of Thermal Sciences and Engineering
November 06th-10th, 2022, Bento Gonçalves - RS - Brazil

ENC-2022-0145
PARALLELIZED NUMERICAL SIMULATION RUN IN GPU FOR THE ANALYSIS OF THE THERMAL EFFECTS IN THE APPLICATION OF DIFFERENT SHIELDING GASES IN AUTOGENOUS WELDING

Arthur Mendonça de Azevedo
Ernandes José Gonçalves do Nascimento
Elisan dos Santos Magalhães
Instituto Tecnológico de Aeronáutica – ITA, São José dos Campos – SP, Brasil
arthurama@ita.br
ernandesn549@gmail.com
elisan@ita.br

Abstract. *Modern-day engineering designs are very sensitive to development and manufacturing costs efficiency. The competitive globalized market prioritizes fast and affordable technological advancements to suit commercial tendencies and avoid obsolescence. The first numerical methods revolution had greatly reduced design costs by requiring fewer experiments to build equivalent devices. However, after nearly fifty years, the application of traditional CPU (Central Processing Unit) based numerical methodology still requires expensive equipment such as processing cluster type computers, room climatization, and higher electricity capacity no-brake systems. The requirement of this high-priced set of machinery gives room for new alternative solutions with higher hardware appliance efficiency. The present work is an example of the application of recent advances in GPU (Graphics Processing Unit) parallel computing, resulting in a faster, less costly, and more reliable numerical methodology. Here, the latest developments and features of an in-house parallelized CUDA-C (Compute Unified Device Architecture) language code were exposed. The software was applied in the analysis of the thermal effects caused by the application of different shielding gases in a simulated autogenous welding process. The heat conduction partial differential equation (PDE) with an added phase-change term is transformed into an algebraic equation and discretized in a three-dimensional domain by the application of the Finite Volume Method (FVM). Additionally, the enthalpy method is applied to account for phase changes in the material by evaluating the drop in temperature due to the latent heat of fusion. Temperature-dependent thermal properties are applied to the welded specimen material. The resultant temperature and material liquid fraction fields were discussed. The simulation outputs were also exposed as a function of shielding gas type. The present research outcomes had suggested that the analyzed methodology has enough potential for replacing traditional CPU (Central Processing Unit) processing techniques, thus greatly reducing costs by minimizing time expenditure and required laboratory apparatus.*

Keywords: *Autogenous welding, Numerical phase change, Finite Volume Method, GPU processing, CUDA-C language.*

1. INTRODUCTION

The application of numerical methods revolutionized engineering design by virtualizing the creational process of a new technology. The use of extensive laboratory experimentation supported by expensive physical apparatus gave room to smaller spaces filled with robust computational structures. The continuously growing use of numerical methods had contributed to a shift from the traditional design techniques to a new digital era focused on hardware and software enhancements for engineering applications. For instance, Xia and Sun (Xia & Sun, 2002) had cited the ability of the numerical methods in predicting the performance of new design processes before they are manufactured or implemented. The authors had also extensively described the advantages of CFD applications: the easier evaluation of geometric changes, elimination of conditional design aspects and the ability of simulating conditions where it is not possible to take detailed measurements, to cite a few. Mrope *et al.* (Mrope, Jande, & Kievele, 2021) added that experimentation is bottle necked by the limited number of quantities that can be measured at a time, while in numerical analysis any desired quantities may be measured at once, with a high resolution in space and time.

The development timeline of computational methods has its beginning in the twentieth century. Richardson (Richardson, 1922) was one of the first scientists to develop and document research on the use of numerical means to predict forecast changes in the weather. The book is considered by many to have set the basis for modern CFD numerical methods. The author had presented unsuccessful calculations with the use of finite differences and spatial divisions in cells, resembling the concepts of a mesh. Following the evolution of numerical methods, Patankar (Patankar, 1980) published one of the earliest remarkable books about modern numerical techniques. The author exposed physical concepts about fluid flow and heat transfer phenomena using simple algebra and elementary calculus. Posteriorly, Crank (Crank, 1984) focused specifically on presenting a detailed account of mathematical and numerical methods to solve free and moving-boundary problems. The book contained a strong list of references, ranging from important mathematical approaches of the nineteenth century until the date of publishing. Ferziger and Perić (Ferziger & Peric, 2002) exemplified coding approaches involving solutions by the Finite Difference Method (FDM) for beginners in numerical methods. The published work also contributed to the solution of the Navier-Stokes equations, grid quality analysis and the modeling of complex geometry problems. Versteeg and Malalasekera (Versteeg & Malalasekera, 2007) exposed didactic applied examples of unsteady and steady state heat conduction, convection, combustion, turbulent fluid flows with pressure – velocity coupling and radiative heat transfer. The published book gives special emphasis to the Finite Volume Method (FVM) with solutions developed mainly in one or two dimensions. Additionally, the authors also dissertated about the basic concepts of specific methods for solving complex geometries. More recently, Moukalled *et al.* (Moukalled, Mangani, & Darwish, 2016) published a work focused on the application of the FVM implemented with OpenFOAM and MATLAB. The book explores two specific CFD codes, being the first a three-dimensional unstructured pressure-based finite volume academic CFD code implemented with MATLAB. The second is an open-source framework implemented in OpenFOAM used in the development of a range of CFD programs for the simulation of industrial scale flow problems.

The works previously cited had made fundamental contributions to the development of computational methods. However, the recent advances in computer architecture requires the adaptation of traditional approaches to better suit cutting edge technology hardware. For instance, Bhadke *et al.* (Bhadke, Kawale, & Inamdar, 2014) developed a GPU-based in-house three-dimensional code focused on solving heat conduction using CUDA. The work was developed using the alternating direction implicit method, which is also known as the splitting method. This approach is an alternative to the Crank-Nicolson method, which is computationally intensive when applied for more than one dimension. The authors obtained a speedup up to 11x, which increases as the size of elementary cells in the grid decreases. Following this line of research, Lai *et al.* (Lai, Yu, Tian, & Li, 2020) developed a turbulent flow study with a hybrid parallel algorithm implemented with Computing Unified Device Architecture (CUDA) running on clusters with multi-GPU High-performance Computing (HPC). The work was performed with the application of the AUSM + UP upwind interpolation scheme and the three step Runge-Kutta discretization method for space and time, respectively. As a result, the authors obtained an acceleration rate of more than 36x that of traditional CPU processing approaches. The research outcomings produced insights that GPU parallelization can greatly overcome the processing velocity of CPU-based parallel computing. Kuo and Wu (Kuo & Wu, 2021) proposed the optimization of a low-level assembly code to reconstruct the flux for a splitting flux Harten-Lax-van Leer (SHLL) scheme on high-end GPUs. The solver was implemented using the weighted essentially non-oscillatory reconstruction method to simulate compressible gas flows derived from an unsteady Euler equation. The parallel code thread execution and instruction set architecture was performed in CUDA. The research resulted in a reduction of 26.7% of floating-point operations and an increase of 37.5% in bandwidth. The authors have achieved 66% of the peak performance for Nvidia v100, which is twice the computing efficiency of the studies previously reported. Furthermore, Ye *et al.* (Ye, Zhang, Wan, & Sun, 2022) made solid attempts in improving the data transfer efficiency between CPU and GPU by proposing a set of hardware-aware technology. The proposed software consisted in an in-house GPU based multiblock structured CFD solver discretized by a high order Finite Difference Method (FDM) on curvilinear coordinates. Additionally, the research compared the accelerating effects achieved using different GPUs. The implements resulted in a speed up of around 2000x over a single CPU core.

Although significant advances had been made recently in the development of parallelized numerical codes, there is still plenty of space to push the evolutionary boundary of this field. The CPU processing techniques have received solid research work for more than fifty years, while GPU processing has barely reached ten years on development. Hence, in the present research, a demonstration of a parallelized numerical simulation run in GPU was performed. A Laser Beam Welding (LBW) process with an automated moving heat source was simulated to exemplify the effectiveness of the implemented parallelized methodology. The results were based on the analysis of the thermal fields resulting from the application of a mixture of argon, helium, carbon dioxide, nitrogen, and oxygen as shielding gases. The simulations were run in an inhouse code developed using CUDA-C language, by Nvidia™, and the SOR (Successive over-relaxation) parallelized solver. The heat conduction partial differential equation (PDE) with an added phase-change term was transformed into an algebraic equation and discretized in a three-dimensional domain by the application of the Finite Volume Method (FVM). Temperature dependent thermal properties were applied to the welded specimen material. The enthalpy method was applied to account for phase changes in the material by numerically calculating the drop in temperature due to the latent heat of fusion. The thermal modeling accounted for radiation and convection losses

outside the position of the welding beam and shield gas flux. The resultant shielding gas thermal effects were compared and discussed by means of the temperature field. The research outcomes had suggested that the applied methodology has enough potential for replacing traditional CPU processing techniques. The parallelization approach employed had demonstrated the capability of significative costs reduction by minimizing time expenditure, computational costs and required laboratory apparatus.

2. BASIC CONCEPTS AND METHODOLOGY

2.1 Laser Beam Welding (LBW) and Shielding Gases

Laser Beam Welding (LBW) shielding gases are a fundamental part of the process of building high-quality welds. However, the effects of shielding gases in optical autogenous welding processes are not clear yet. It is well known that it can prevent the weld from oxidation in some cases, but it may also cause defocusing of the beam of laser light in the plasma plume directly above the laser-generated keyhole (Glowacki, 1995). The application of local gas flow in LBW also affects the pressure balance inside the keyhole and therefore, its stability. For instance, previous investigations had demonstrated a reduction in spatter and pore formation for partial penetration welding up to a speed of 5 m/min (Schmidt, Schricker, Bergmann, & Junger, 2020). Adding to these issues, the argon type shielding gas is one of the cheapest and most widely used but faces the problem of plasma generation depending mainly on the laser power and other welding conditions (Watanabe, Nakbayashi, Hiraga, Inoue, & Matsunawa, 1999).

The mapping of LBW welding process parameters and corresponding thermal effects are an extensive task due to the number of variables involved. For example, Motlagh *et al.* (Motlagh, Parvin, Jandaghi, & Torkamany, 2013) found that for a mixture of helium and argon shielding gases, the loss of light beam power depends on the laser wavelength and the plasma plume characteristics (plasma temperature and density electron). However, the effects may change dramatically just by removing one of the shielding gas components (helium or argon) or by changing the applied type of gas. In fact, Elmer *et al.* (Elmer, Vaja, Carlton, & Pong, 2015) reported that complete, or near complete elimination of porosity in 304L stainless steel keyhole laser welds was obtained when using N_2 instead of Ar shielding gas. Hence, the particularities of any combination of shielding gases parameters are unique and efforts made to model, simulate, and map the thermal effects are of fundamental importance to the laser welding community.

2.2 Mathematical Modeling

The applied heat conduction model is composed of the non-linear three-dimensional heat diffusion differential equation, with phase change modeling performed through an enthalpy function. The mathematical modeling may be represented as:

$$\frac{\partial}{\partial x}\left(\lambda\frac{\partial T}{\partial x}\right)+\frac{\partial}{\partial y}\left(\lambda\frac{\partial T}{\partial y}\right)+\frac{\partial}{\partial z}\left(\lambda\frac{\partial T}{\partial z}\right)+\dot{g}=\frac{\partial H}{\partial t} \tag{1}$$

where x, y and z are the cartesian coordinates, λ is the non-linear thermal conductivity, T is the numerical temperature, $\dot{g}$ is the volumetric heat source, t is the time and H is the total enthalpy density, which may be written as (Crank, 1984),

$$H=\rho\int_0^T c_p\left(\phi\right)d\phi+\rho f\left(T\right)L \tag{2}$$

where ρ is the density, c_p is the specific heat at constant pressure, ϕ is the integration variable, L is the latent heat of fusion and f is the Heaviside step function, which is expressed as:

$$f=\begin{cases}1 \text{ if } T<T_m\\ 0 \text{ if } T>T_m\end{cases} \tag{3}$$

where T_m is the temperature of fusion.

The specimen was subjected to forced and natural convection and radiation. The first of them was caused by the shielding gas flow, which moved with the LBW heat source. This work considered the forced convection in the modeling of the shielding gas influence, which is assumed to be like a Single Round Nozzle (Martin, 1977). Additionally, the radiation of the specimen was also considered. Therefore, this boundary condition can be written as:

$$-k\left.\frac{\partial T}{\partial y}\right|_{y=L_y} = \bar{h}\left(T - T_g\right) + \boldsymbol{\sigma\varepsilon}(T)\left(T^4 - T_\infty^4\right) \tag{4}$$

with:

$$\bar{h} = \frac{\overline{N_{u,D_g}}\,k_g}{D_g} \tag{5}$$

$$\overline{N_{u,D_g}} = \mathbf{Pr}_g^{0.42}\,\frac{D_g}{r}\,\frac{1.0 - 1.1\dfrac{D_g}{r}}{1.0 + 0.1\left(\dfrac{H_g}{D_g} - 6.0\right)\dfrac{D_g}{r}}\,F\left(\mathbf{Re}_g\right) \tag{6}$$

$$F(\mathbf{Re}_g) = 2\,\mathbf{Re}_g^{0.5}\left(1.0 + \frac{\mathbf{Re}_g^{0.55}}{200.0}\right)^{0.5} \tag{7}$$

$$\mathbf{Re}_g = \frac{u_g D_g}{\boldsymbol{\nu}_g} \tag{8}$$

where σ is the Stefan Boltzmann constant, ε is the material's emissivity, T_g is the gas temperature, T_∞ is the ambient air temperature, $\bar{h}$ is the average heat transfer coefficient. For the shielding gas, $\overline{N_{u,D_g}}$ is the average Nusselt number, k_g is the gas thermal conductivity, D_g is the diameter of the round nozzle, Pr_g is the Prandtl number, r is the radial coordinate, H_g is the distance between the nozzle exit and the north surface of the specimen, $F(Re_g)$ is the Reynolds function, Re_g is the Reynolds number, u_g is the velocity, and v_g is the kinematic viscosity. For the properties of the shielding gas (k_g, Pr_g and v_g), the authors considered the film temperature, with the average temperature of the weld region and the environment temperature. Hence,

$$T_{film} = \frac{T_{avg} + T_\infty}{2} \tag{9}$$

The LBW heat source modeling is shaped as a gaussian conical volumetric heat distribution, as exposed in Fig. Figure **1**. The mathematical description of the moving heat source is given as (Magalhães, 2021):

$$\dot{g} = \frac{Q_W}{0.460251 h_p R^2}\,e^{-\frac{4.5(z-ut)^2}{R^2}}\,e^{-\frac{4.5\left(y-L_y/2\right)^2}{R^2}}\left(1 - \frac{x^{1/2}}{h_p^{1/2}}\right) \tag{10}$$

where Q_w is the LBW power, h_p is the height of penetration, R is the welding radius and u is the welding head velocity.

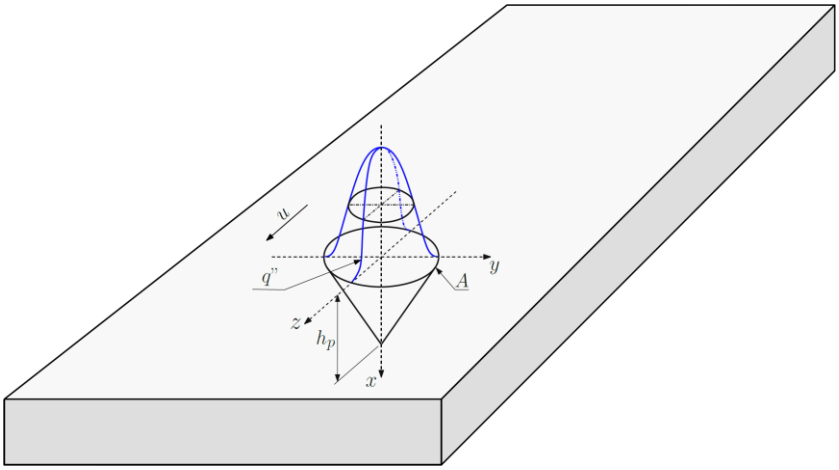

Figure 1. Applied Gaussian conical volumetric heat distribution.

2.3 Simulation Domain, Parameters and Material Properties

The domain of solution of Eq. (1) is represented in Figure 2. The measurements L_x, L_y and L_z are the domain dimensions in the x, y and z directions, Q_w is the heat input from the welding head source, Q_{rad} is the heat loss by radiation and Q_{con} is the heat loss by convection.

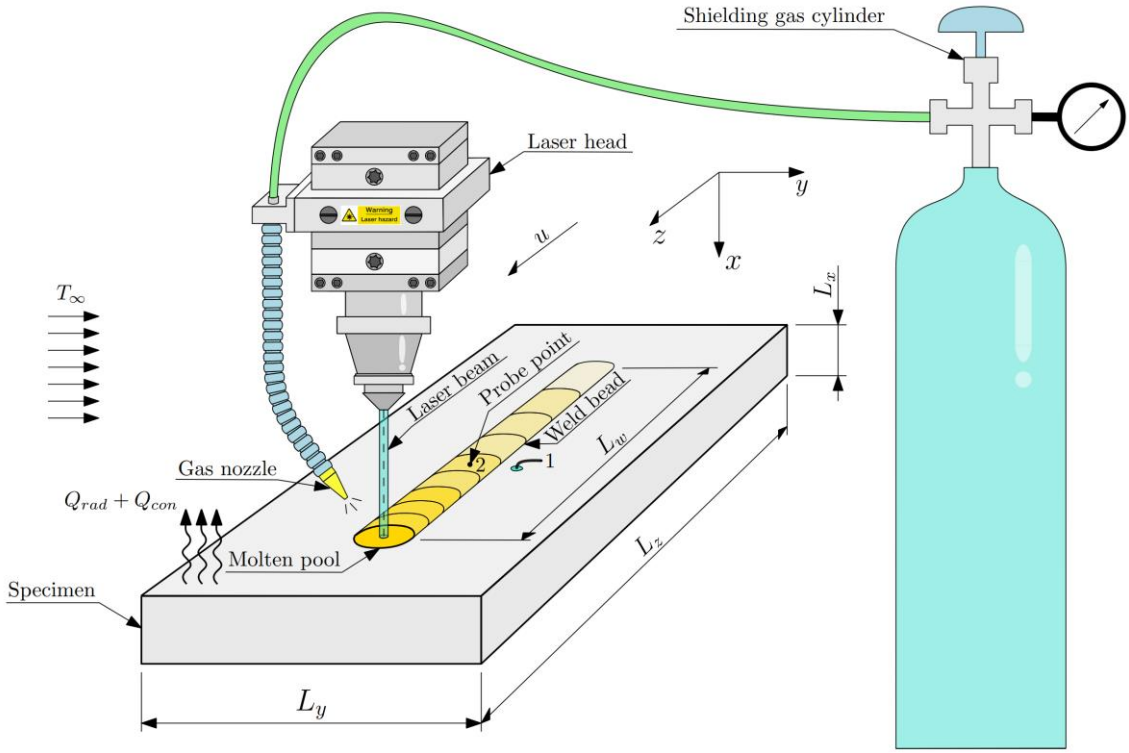

Figure 2. Simulated LBW process with shielding gas nozzle.

The welded material was a SAE 1020 steel sample. The simulated physical apparatus was composed of a fiber laser power source of 3000 W. The values for the weld penetration and bead radius are h_p = 1.91 mm and R = 0.5 mm, respectively. The applied melting temperature was 1450.0 ºC. Table 1 presents the additional simulation parameters, and SAE 1020 steel thermal properties. In addition, this work considered eight gas combinations, such as 100% Ar, 100% He, 75% Ar + 25% He, 50% Ar + 50% He, 100% CO_2, 80% Ar + 20 CO_2, 100% N_2, 80% Ar + 20% N_2, and 88% Ar + 12% O_2. Furthermore, the authors considered the weighted mean for the thermal properties of these combinations, neglecting the interaction between the gases. Table 2 presents the range of the thermal properties of shielding gases.

Table 1. Simulation parameters, and SAE 1020 steel thermal properties.

Parameter	**Values**
L_x, L_y, L_z and L_w [mm]	9.5, 31.0, 70.0 and 45.0
u [m/s]	0.05
Thermal properties (SAE 1020)	**Values / Equations**
λ [W/m.K]	$2.5 \times 10^{-5}T^2 - 0.053T + 57.2$
c_p [J/kg.K]	$2.78e^{1.19 \times 10^{-3} T}$
ε	0.8
ρ [kg/m³] and L [kJ/kg]	7870.0 and 250.0
Parameter (Shielding gas)	**Values**
u_g [L/min]	15.0
D_g [mm]	10.0
H_g [mm]	300.0
T_q [°C]	-0.94

Table 2. Shielding gas thermal properties.

Gas and mixtures	**Variable Properties**		
	Pr	λ_g **[W/m.K]**	v_g **[m²/s]**
100% Ar	0.668 – 0.669	0.012 – 0.089	6.55×10^{-6} – 7.06×10^{-4}
100% He	0.666 – 0.672	0.117 – 0.778	6.21×10^{-5} – 6.21×10^{-3}
75% Ar + 25% He	0.667 – 0.670	0.039 – 0.261	2.04×10^{-5} – 2.08×10^{-3}
50% Ar + 50% He	0.667 – 0.671	0.065 – 0.434	3.43×10^{-5} – 3.45×10^{-3}
100% CO_2	0.784 – 0.028	0.012 – 4.17	5.80×10^{-6} – 4.73×10^{-4}
80% Ar + 20% CO_2	0.687 – 0.540	0.013 – 0.904	6.83×10^{-6} – 6.26×10^{-4}
100% N_2	0.737 – 0.760	0.018 – 0.150	7.54×10^{-6} – $7,62 \times 10^{-4}$
80% Ar + 20% N_2	0.681 – 0.687	0.014 – 0.101	6.70×10^{-6} – 7.14×10^{-4}
88% Ar + 12% O_2	0.676 – 0.677	0.013 – 0.098	6.64×10^{-6} – 4.73×10^{-4}

A grid size independence study has demonstrated that the simulation outputs became independent of mesh refinement at 1,500,000 total nodes. Therefore, the problem was simulated with a nonuniform structured mesh size of 1,750,100 total nodes. A time-step size independence analysis with fixed values was also addressed. Results became independent of temporal grid refinement for values smaller than 10^{-2} s. As a result, a time-step size of 10^{-3} s was applied.

3. RESULTS AND DISCUSSION

This work determined all the numerical solutions considering an in-house parallelized CUDA-C code. An Nvidia Geforce GTX 1660 Ti 6GB card processed these codes.

First, the experimental verification of the LBW considered the thermocouple 1, as presented in Figure 2. Furthermore, the experimental setup used 100% Argon as shielding gas in this case. Figure 3 presents the experimental results for the thermocouple 1 and the numerical simulation for this point and the probe point 2 (Figure 2). The agreement between the dashed and the green curve validated the in-house code for the heating and cooling processes of the LBW simulation.

Furthermore, this paper appraised the numerical simulation at the thermocouple (1) and the probe point (2), as indicated in Figure 2, for the shielding gases test and comparison. Figure 4 – 7 show these comparisons. In tests with the thermocouple 1, the differences with the shielding gases were insignificant. The comparison between 100% Ar and 100% He was the one with the most significant disparity, 0.74% difference (Figure 4a). In contrast, the other mixtures with CO_2 (Figure 5a), N_2 (Figure 6a), and O_2 (Figure 7a) presented the same simulation result of the model with shielding gas composed of 100% Ar. On the other hand, the probe point 2 simulation results showed some significant differences. The shield gas is composed of 100% He presented a 2% difference for the gas with 100% Ar (Figure 4b). As expected, as the Helium concentration decreased, this difference was smaller, reaching 0.6% for the gas with 75% Ar + 25% He. For the case with 100% N_2 (Figure 6b), this difference was 0.4%, which decreased with the reduction of N_2 concentration. Despite these disparities, even in the weld pool, the simulations with Argon mixed with Carbon

Dioxide (Figure 5b) and Oxygen (Figure 7b) showed insignificant residues when compared to the model solution with 100% Ar.

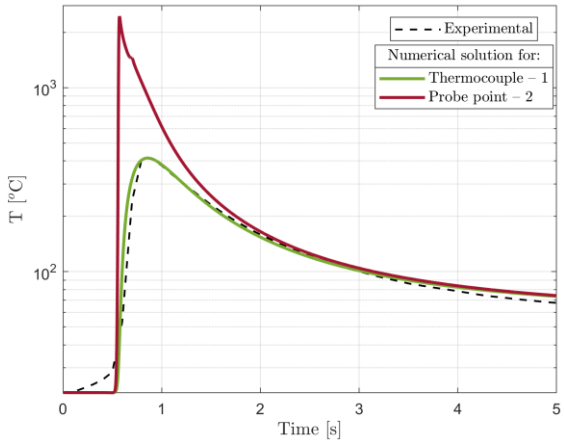

Figure 3. Experimental results for the thermocouple 1 and numerical simulation for the thermocouple 1 and the probe point 2.

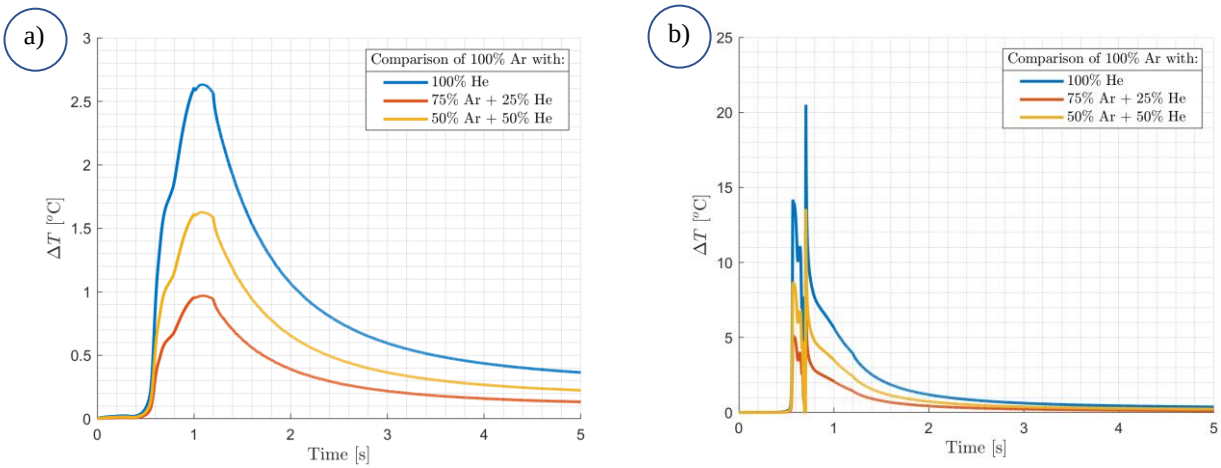

Figure 4. Comparison between 100% Ar with 100% He, 75% Ar + 25% He, and 50% Ar + 50% He at a) thermocouple 1, and b) probe point 2.

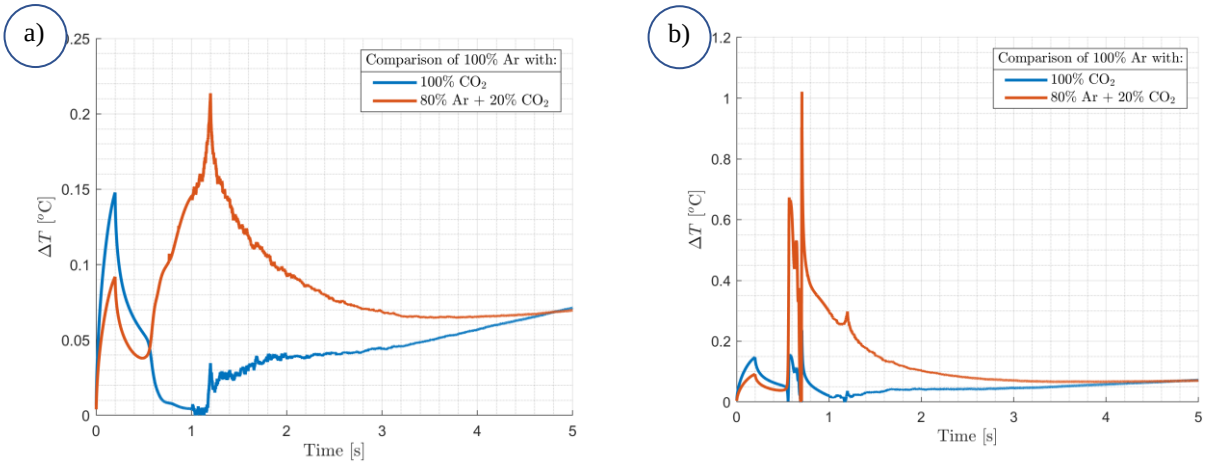

Figure 5. Comparison between 100% Ar with 100% CO_2, and 80% Ar + 20% CO_2 at a) thermocouple 1, and b) probe point 2.

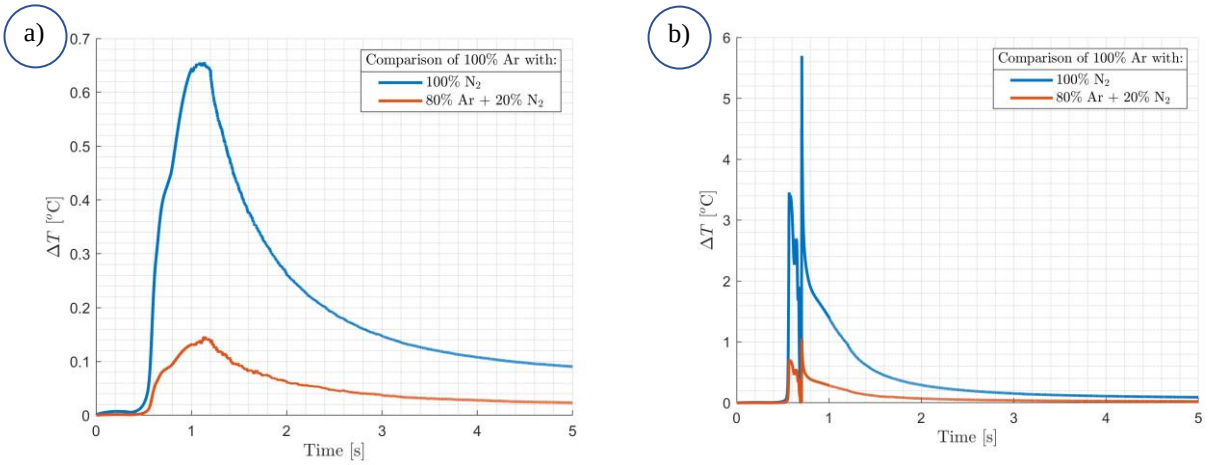

Figure 6. Comparison between 100% Ar with 100% N_2, and 80% Ar + 20% N_2 at a) thermocouple 1, and b) probe point 2.

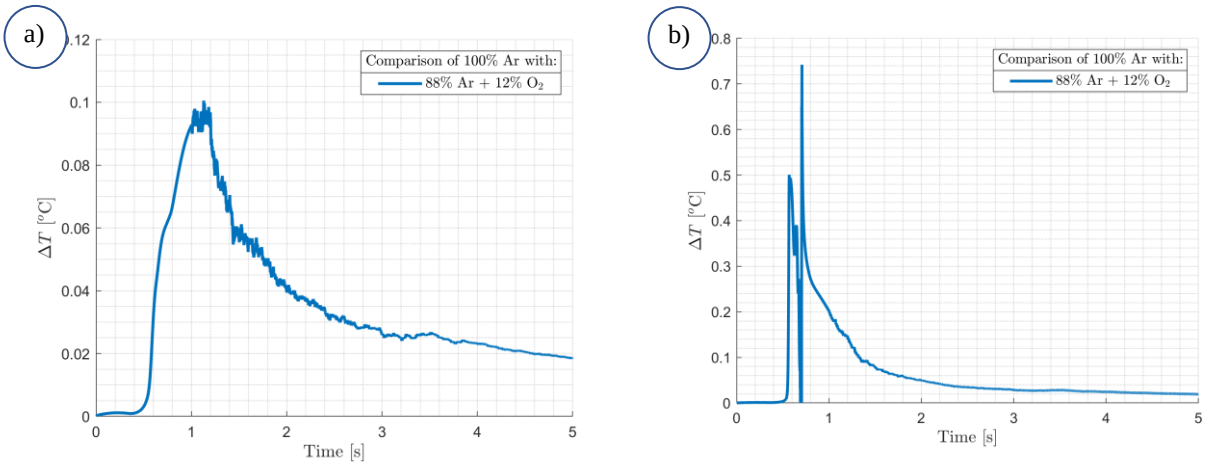

Figure 7. Comparison between 100% Ar with 88% Ar + 12% O_2 at a) thermocouple 1, and b) probe point 2.

4. CONCLUSION

This work presented the LBW simulation with 100% Argon shielding gas and compared the numerical and experimental results. The simulations focused on analyzing the thermal fields resulting from applying a mixture of argon, helium, carbon dioxide, nitrogen, and oxygen as shielding gases. Furthermore, this approach demonstrated the ease of use of different shielding gas mixtures without specific laboratory apparatus. Therefore, it is considered cheap and useful as the initial analysis for shield gas choice. Finally, the parallelization methodology has enough potential to replace traditional techniques, such as CPU processing.

5. REFERENCES

Bandarra Filho, E.P. and Jabardo, J.M.S., 2011. "Convective boiling performance of refrigerant R-134a in herringbone and microfin copper tubes". *International Journal of Refrigeration*, Vol. 29, No. 1, pp. 81–91.

Bhadke, Y. D., Kawale, M. R., & Inamdar, V. (2014). Development of 3D-CFD code for Heat Conduction Process using CUDA. *IEEE International Conference on Advances in Engineering & Technology Research* (pp. 1 - 5). Unnao, India: ICAETR - 2014.

Cavalini Junior, A.A., 2013. *Detecção e identificação de trincas transversais incipientes em eixos horizontais flexíveis de máquinas rotativas*. Ph.D. thesis, Universidade Federal de Uberlândia, Uberlândia, Brasil.

Cavalini Junior, A.A., Lara-Molina, F.A., Sales, T.P., Koroishi, E.H. and Steffen, V., 2015. "Uncertainty analysis of a flexible rotor supported by fluid film bearings". *Latin American Journal of Solids and Structures*, Vol. 12, pp. 1487–1504.

Crank, J. (1984). *Free and Moving Boundary Problems.* Oxford, UK: Oxford University Press.

Elmer, J. W., Vaja, J., Carlton, H. D., & Pong, R. (2015). The Effect of Ar and N2 Shielding Gas on Laser Weld Porosity in Steel, Stainless Steels, and Nickel. *Supplement to the Welding Journal*, 313 - 325.

Ferziger, J. H., & Peric, M. (2002). *Computational methods for fluid dynamics.* New York: Springer.

Glowacki, M. H. (1995). The effects of the use of different shielding gas mixtures in laser welding of metals. *Journal of Physics D: Applied Physics*, 2051 - 2059.

Kuo, F. A., & Wu, J. S. (2021). Implementation of a parallel high-order WENO-type Euler equation solver using a CUDA PTX paradigm. *Journal of Mechanics*, 496 - 512.

Lai, J., Yu, H., Tian, Z., & Li, H. (2020). Hybrid MPI and CUDA parallelization for CFD applications on multi-GPU HPC clusters. *Scientific Programming*.

Magalhães, E. S. (2021). A quadrilateral optimization method for non linear thermal properties determination in materials at high temperatures. *International Journal of Heat and Mass Transfer*, 1 - 10.

Martin, H. (1977). *Heat and mass transfer between impinging gas jets and solid surfaces.* New York: Academic Press.

McConnell, K.G. and Varoto, P.S., 2008. *Vibration Testing: Theory and Practice*. John Wiley & Sons, New Jersey, 2nd edition.

MLA, 2004. "How do I document sources from the web in my works-cited list?" Modern Language Association. 22 Feb. 2007 <http://www.mla.org>.

Motlagh, N. H., Parvin, P., Jandaghi, M., & Torkamany, M. J. (2013). The influence of different volume rations of He and Ar in shielding gas mixture on the power waste parameters for Nd:YAG and CO2 laser welding. *Optics & Laser Technology*, 191 - 198.

Moukalled, F., Mangani, L., & Darwish, M. (2016). *The Finite Volume Method in Computational Fluid Dynamics: An Advanced Introduction with OpenFOAM and MATLAB.* New York: Springer International Publishing.

Mrope, H. A., Jande, Y. A., & Kievele, T. T. (2021). A Review on Computational Fluid Dynamics Applications in the Design and Optimization of Crossflow Hydro Turbines. *Journal of Renewable Energy*, 1 - 13.

Patankar, S. V. (1980). *Numerical Heat Transfer and Fluid Flow.* Boca Raton: CRC Press.

Richardson, L. F. (1922). *Wather Prediction by Numerical Process.* Cambridge, UK: Cambridge Mathematical Library.

Santos, D.D., Furtado, G.M., Frey, S.L., Naccache, M.F. and de Souza Mendes, P.R., 2013a. "Flow of elasto-viscoplastic fluids inside a cavity". In *Proceedings of the 22nd International Congress of Mechanical Engineering - COBEM 2013*. Ribeirão Preto, Brazil.

Santos, D.D., Furtado, G.M., Frey, S.L., Naccache, M.F. and de Souza Mendes, P.R., 2013b. "Numerical investigation of elastic and viscous effects on inertial viscoplastic fluid flows". *In Proceedings of the 22nd International Congress of Mechanical Engineering - COBEM 2013*. Ribeirão Preto, Brazil.

Schmidt, L., Schricker, K., Bergmann, J. P., & Junger, C. (2020). Effect of Local Gas Flow in Full Penetration Laser Beam Welding with High Welding Speeds. *Applied Sciences*, 1 - 19.

Versteeg, H. K., & Malalasekera, W. (2007). *An Introduction to Computational Fluid Dynamics* (2nd ed. ed.). Harlow, England: Pearson Education Limited.

Watanabe, M., Nakbayashi, T., Hiraga, H., Inoue, T., & Matsunawa, A. (1999). Effect of shielding gas plasma on monitoring signals in laser welding: features of monitoring methods for laser welding and their application. *Welding International*, 9 - 20.

Xia, B., & Sun, D.-W. (2002). Applications of computational fluid dynamics (CFD) in the food industry: a review. *Computers and electronics in agriculture, 34*, 5 - 24.

Ye, C.-C., Zhang, P.-J.-Y., Wan, Z.-H., & Sun, D.-J. (2022). Accelerating CFD simulation with high order finite difference method on curvilinear coordinates for modern GPU clusters. *Advances in Aerodynamics*, 1 - 32.

6. ACKNOWLEDGMENTS

The authors would like to thank PETROBRAS, CAPES and CNPq, Brazil, for their invaluable financial support.

7. RESPONSIBILITY NOTICE

The authors are the only responsible for the printed material included in this paper.